Applied Clay Science 182 (2019) 105276

Contents lists available at ScienceDirect

Applied Clay Science

journal homepage: www.elsevier.com/locate/clay

Research Paper

Co(II) impregnated Al(III)-pillared montmorillonite–Synthesis, characterization and catalytic properties in Oxone® activation for dye degradation

Marija Marković[a,b], Sanja Marinović[c,*], Tihana Mudrinić[c], Marija Ajduković[c], Nataša Jović-Jovičić[c], Zorica Mojović[c], Jovana Orlić[d], Aleksandra Milutinović-Nikolić[c], Predrag Banković[c]

[a] University of Belgrade, Faculty of Technology and Metallurgy, Karnegijeva 4, 11000 Belgrade, Republic of Serbia
[b] Serbian Armed Forces, Republic of Serbia
[c] University of Belgrade, Institute of Chemistry, Technology and Metallurgy, National Institute, Center for Catalysis and Chemical Engineering, Njegoševa 12, 11000 Belgrade, Republic of Serbia
[d] Innovation Centre of Faculty of Chemistry, University of Belgrade, Faculty of Chemistry, Studentski trg 12-16, 11000 Belgrade, Republic of Serbia

ARTICLE INFO

Keywords:
Pillared montmorillonite
Cobalt impregnation
Oxone®
Advanced oxidation process
Dye degradation

ABSTRACT

Aluminum pillared clay was synthesized and impregnated with Co^{2+} (CoAP), using incipient wetness impregnation method. The obtained CoAP was characterized by chemical analysis, XRPD, SEM with EDS, XPS and low temperature N_2 physisorption. By these methods the incorporation of Co^{2+} was confirmed in both micro and mesoporous region. The synthesized material was investigated as a catalyst in catalytic oxidation of organic water pollutants – dyes – in the presence of Oxone® (peroxymonosulfate). Oxone® is a precursor of sulfate radicals. Tartrazine was chosen as a model dye pollutant. The influence of the mass of the catalyst, temperature and initial pH was investigated. Temperature increase was beneficial for dye degradation rate. The reaction rate was the highest for initial pH values around those corresponding to neutral conditions, somewhat slower for pH $<$ 4 values, while for pH $>$ 10 decolorization was significantly less expressed. Along with decolorization of tartrazine solution the formation and degradation of tartrazine catalytic oxidation products were monitored using UV–Vis spectroscopy. CoAP was found to be efficient catalyst in Oxone® induced catalytic degradation of both tartrazine and detected products of its degradation.

1. Introduction

In the broadest sense, advanced oxidation processes (AOP) comprise aqueous phase oxidation methods involving highly reactive species that can react with organic contaminants in water (Kommineni et al., 2008). Oxidation processes involving sulfate radicals, as strong oxidants, have received much attention recently (Yang et al., 2015). Peroxymonosulfate (PMS) can be used as a precursor of sulfate radicals. It is regarded as an environmentally friendly oxidant. Without outer activation PMS very slowly decomposes into $SO_4^{\cdot -}$ radicals (Chen et al., 2018). PMS can be activated in different ways, using heat, metal ions and UV irradiation (Durairaj et al., 2018; Ahn et al., 2016; Ahmad et al., 2013; Verma et al., 2016). Among these methods, the activation of PMS by transition metals has attracted much attention because of high activation efficiency of transition metals (Chen et al., 2018). Many researchers have been investigated transition metal activation of peroxymonosulfate in catalytic oxidation processes. Co^{2+}, Mn^{2+}, Ni^{2+}, Fe^{2+}, Ru^{3+} and so forth, have been proven as successful catalysts for PMS activation (Hu and Long, 2016; Oh et al., 2016).

Among these transition metal ions, cobalt (Co^{2+}) is considered to be the most effective activator of PMS (Anipsitakis and Dionysiou, 2004; Nfodzo and Choi, 2011). Ball and Edwards were the first who used cobalt for the catalytic decomposition of peroxymonosulfate (Ball and Edwards, 1956; Ball and Edwards, 1958). System consisting of Co^{2+} and PMS might be regarded as an alternative to the Fenton's reaction system. Higher oxidation potential of sulfate radical (2.5–3.1 eV) comparing to that of hydroxyl radical (2.7 eV) leads to faster reaction rate in oxidation processes (Shukla et al., 2011). However, the major problem in homogeneously catalyzed decomposition of peroxymonosulfate using Co^{2+} as catalyst is the toxicity (ATSDR, 1992) and

* Corresponding author at: Njegoševa 12, 11000 Belgrade, Republic of Serbia.
E-mail address: sanja@nanosys.ihtm.bg.ac.rs (S. Marinović).

https://doi.org/10.1016/j.clay.2019.105276
Received 6 June 2019; Received in revised form 21 August 2019; Accepted 22 August 2019

difficulty of recovering of cobalt ions. In order to restrict the discharge of cobalt ions, several attempts have been made to obtain heterogeneous cobalt catalyst where cobalt is supported on a solid support. Different supports for cobalt ions have been investigated (Hu and Long, 2016; Yang et al., 2007; Yang et al., 2008; Huang et al., 2017).

Pillared interlayered clays (PILCs) represent materials with permanent micro and/or mesoporosity, and thermal and chemical stability with great catalytic potential (Herney-Ramírez and Madeira, 2010; Mishra, 2010; Baloyi et al., 2018). PILC catalysts can be tailored by alternating the final properties of PILCs. This can be achieved by choosing different types of clay and particle sizes, nature of the pillaring agent, pillaring procedure and thermal treatments. One of the methods of the preparation of PILCs comprises ion exchange of interlamellar cations by the polyhydroxy cations. Intercalated polyhydroxy cations increase the basal spacing of the clay. Upon calcination, the dehydration and dehydroxylation of intercalated species occurs and they are converted into oxide pillars that expand interlamellar spacing (Herney-Ramírez and Madeira, 2010). After calcination, the resulting PILCs exhibit a regular layered structure, loss of swelling, surface acidity, and increased surface area.

PILCs are reported as promising catalysts with a broad range of applications, one of which is as active catalysts in oxidation reactions of environmental interest (Khelifi et al., 2016). Another important application of PILCs is their use as support for active catalytic phases in the preparation of supported catalysts. This application of PILCs is particularly important in environmentally friendly reactions (Gil et al., 2008). Cobalt impregnated pillared clays have not been extensively investigated as cobalt based catalysts for AOP. Therefore, cobalt, as a catalytically active species, can be introduced to PILC by impregnation using the incipient wetness impregnation procedure (Pinna, 1998).

Potassium peroxymonosulfate (Oxone®, $KHSO_5{\cdot}0.5KHSO_4{\cdot}0.5K_2SO_4$) has been widely used in catalytic oxidation processes as a source of peroxymonosulfate ions (HSO_5^-) that yield $SO_4^{\cdot -}$ radicals during catalytic decomposition in the presence of transitional metals. Oxone® is the most effectively activated by transition metal cations, with cobalt exhibiting the best performance (Hu and Long, 2016; Lin et al., 2017; Lin et al., 2018; Anipsitakis et al., 2005).

Cobalt/ Oxone® systems have proven to be effective in the catalytic oxidation process of different organic contaminants in waste waters; such are azo dyes (Lin et al., 2017; Lin and Lin, 2018).

In this study aluminum pillared clay was synthesized and impregnated with cobalt, using incipient wetness impregnation method. The obtained PILC was characterized and investigated as a catalyst in catalytic oxidation of tartrazine, as model dye pollutant in wastewaters. Synthetic dyes are harmful and toxic to environment and human being (Hajjaji et al., 2016).Tartrazine was selected for this study as an azo dye which is used in food, cosmetics, pharmaceuticals and textile industry (Jain et al., 2003). Tartrazine shows high stability against biodegradation and conventional wastewater treatments of industrial effluents. (Chekir et al., 2017). The influence of mass of the catalyst, temperature and initial pH on tartrazine decolorization and degradation was investigated here.

2. Materials and methods

2.1. Materials

Clay used in pillaring procedure was purchased from The Source Clays Repository - The Clay Minerals Society, Wyoming, USA. The 2 μm fraction (SWy-2) (CMS, 2019) was obtained by hydroseparation and Na-exchanged using common procedure (Mudrinić et al., 2014) (Na-Wy).

All chemicals used in this work were analytical grade. NaCl and NaOH were supplied by Moss Belgrade, $Al(NO_3)_3 \times 9H_2O$ by Kemika Zagreb, $Co(NO_3)_2 \times 6H_2O$ by Centrohem Belgrade. Oxone® (potassium peroxymonosulfate, $KHSO_5{\cdot}0.5{\cdot}KHSO_4{\cdot}0.5{\cdot}K_2SO_4$–Sigma Aldrich) and tartrazine (Sigma Aldrich, ≥85% purity) were used as received.

2.2. Synthesis

Na-Wy was dispersed in distilled water and used in pillaring process (Kaloidas et al., 1995). Pillaring procedure comprised the preparation of pillaring solution with OH^-:Al^{3+} = 2.0 M ratio (100 mmol:50 mmol), obtained by dropwise addition of 500 cm^3 of 0.2 mol dm^{-3} NaOH solution into 250 cm^3 of 0.2 mol dm^{-3} $Al(NO_3)_3$ solution. Thus obtained solution was stirred at 60 °C for 3 h and overnight at room temperature. The pillaring solution was then added dropwise into Na-Wy dispersion (20 g dm^{-3}) in distilled water. The Al^{3+}:Na-Wy ratio was 10 mmol Al^{3+}/g. The suspension was then stirred at 80 °C for 3 h and at 25 °C overnight. After the synthesis procedure, the obtained sample was rinsed by dialysis using deionized water until it was NO_3^- free (tested using UV–Vis spectrophotometry), dried overnight at 110 °C and finally calcined at 300 °C for 2 h. The resulting pillaring clay was referred to as AP.

Incipient wetness impregnation method was used for Co^{2+} impregnation of AP (El-Bahy et al., 2008). The impregnation was performed by slow addition of 0.494 cm^3 of 1.0 mol dm^{-3} Co^{2+} solution introduced by means of impregnation to AP powder resulting in 0.029 g Co^{2+} per 1 g of AP. After drying at 85 °C for 2 h and at 110 °C overnight the calcination at 450 °C for 6 h was applied. The sample was denoted CoAP.

2.3. Characterization

Two X-ray powder diffractometers equipped with a Cu anode (λ = 0.1542 nm) were used to obtain X-ray powder diffraction (XRPD) patterns of Na-Wy, AP and CoAP. First Philips PW 1710 was used in the 2θ interval from 3° to 70° with the step of 0.02°. The reflection corresponding to 001 planes was observed for all the materials, however present but not sufficiently distinguished in the case of CoAP. Hence, another XRPD analysis was required to be performed, using higher sensitivity equipment. This time the diffractograms were recorded in the 2θ range from 2° to 25° using a Rigaku SmartLab (with low background Si-support; 1D Plex 250 Ultra detector and speed 1°/min).

The chemical composition of the samples was determined using the wavelength dispersive X-ray fluorescence spectroscopy (XRF). An ARL™ PERFORM'X Sequential X-Ray Fluorescence Spectrometer (*Thermo Fisher Scientific*) was equipped with a 4.2 kW Rh X-ray tube. For qualitative analysis, spectral recording and data treatment, the Thermo Scientific™ OXSAS software was used (Thermofisher, 2019a). The ARL UniQuant software was used for quantitative data analysis (Thermofisher, 2019b; Gržetić et al., 2016). Moisture content in the samples was estimated using Electronic Moisture Balance (Kern MLB_N, Kern & Sohn Gmbh) and used as input data in Uniquant calculations.

Nitrogen adsorption–desorption isotherms were determined using a Sorptomatic 1990 Thermo Finnigan at −196 °C. The samples were outgassed at 160 °C for 20 h. Obtained isotherms were analyzed applying various models included in the WinADP software. Total pore volume, $V_{0.98}$, was calculated according to the Gurvitsch method. Specific surface area, S_{BET}, was calculated according to the three parameter Brunauer, Emmett and Teller method. The *t*-plot method was applied in order for micropores' surface area from external surface area to be distinguished. As a standard reference *t*-curve the Harkins and Jura relation was used. Mesopore diameter distribution curves were obtained according to the Barrett, Joyner, Halenda method (Gregg and Sing, 1967; Rouquerol et al., 1999; Webb and Orr, 1997; Dubinin, 1974; Scherdel et al., 2010).

A Spectro Spectroflame M – inductively coupled plasma optical emission spectrometer (ICP–OES) – was used to determine potential leaching of Co^{2+} from the catalyst.

UV–Vis spectra were recorded using a Thermo Scientific Evolution 220 UV–Visible Spectrophotometer in the wavelength range from 200 nm to 600 nm.

For morphological study the Scanning Electron Microscopy (SEM) was used. SEM microphotographs were obtained using a JSM–6610LV

microscope equipped with a device for energy-dispersive X-ray spectroscopy (EDS) with detector X-Max Large Area Analytical Silicon Drift connected with INCA Energy 350 Microanalysis System. The samples were previously gold-coated under vacuum in a Leica EM SCD005 device.

In order for cobalt oxidation state to be confirmed the X–ray photoelectron spectroscopy (XPS) using a VG ESCALAB II electron spectrometer was used.

2.4. Catalytic tests

The catalytic test was performed by stirring aqueous tartrazine solution ($C_{0,dye}$ = 50 mg dm^{-3}) in the presence of 0.130 mmol Oxone® previously established as the most adequate (Marković et al., 2018). The tests were conducted in a 500 cm^3 Pyrex reactor thermostated using a Julabo MC 4 circular heater and equipped with a mechanical stirrer. The following experimental parameters were investigated. The mass of CoAP catalyst varied in the (5–200) mg range, the temperature was in the range (30–70) °C and pH in the interval from 2 to 11. The catalyst was added to the reaction mixture 5 min after the Oxone® was introduced into the tartrazine solution. This moment was taken as the initial (0 min) moment of the reaction. With the respect to this moment aliquots were taken at predetermined periods of time. Supernatant solutions were separated from the solid phase by centrifugation at 17000 rpm for 3 min and analyzed using UV–Vis spectrophotometry. By deconvolution of recorded UV–Vis spectra, previously established characteristic tartrazine UV absorption peaks (Marković et al., 2018) at 231, 257, 275, 370 and 426 nm, were monitored and analyzed. The deconvolution of each spectrum was performed using the MagicPlot Pro 2.7.2 software.

3. Results and discussion

3.1. Results of characterization

The chemical composition of the samples was obtained using XRF method and presented in Table 1. Only cation oxides in the amounts ≥1.0 mass % are presented. Prior to XRF analysis, H_2O content was estimated using electronic moisture balance (Table 1).

As expected, pillaring with aluminum led to the increase of Al_2O_3 content in the analyzed AP in comparison to that of Na-Wy. On the other hand Na^+ in the interlamellar space was replaced by aluminum containing pillars and the amount of Na_2O dramatically decreased in the pillared samples. The hydration of samples decreased in the following order Na-Wy > AP > CoAP. The presence of cobalt was confirmed only in the Co^{2+}-impregnated pillared clay.

XRPD patterns (Fig. 1) enabled the identification of the following phases in all investigated samples: montmorillonite, quartz and feldspar (JCPDS, 1990).

Since the most prominent reflections for cobalt oxides (Co_3O_4, Co_2O_3 and different forms of CoO i.e. hexagonal, monoclinic and cubic) (JCPDS, 1990) are in the range of 2θ from 32° to 39° where can overlap with reflection corresponding to 105 montmorillonite reflection, the XRPD spectrum was recorded up to 2θ = 70° in order to detected additional reflections corresponding to cobalt oxides. Nevertheless, no forms of cobalt oxide were identified. Probably, the amount of cobalt

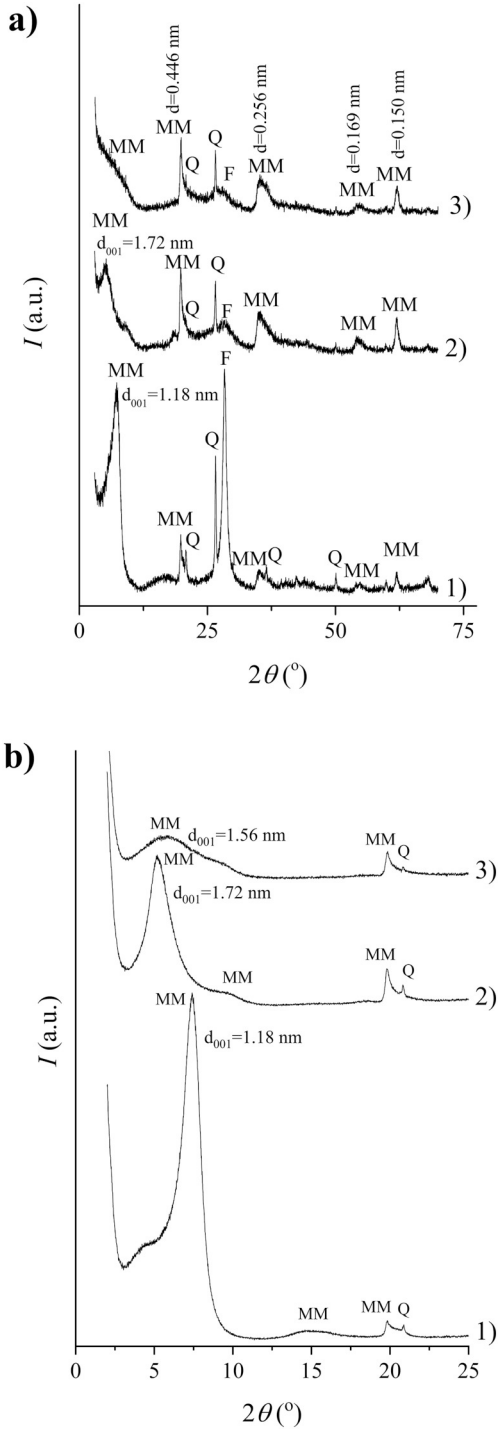

Fig. 1. X-ray diffraction patterns of samples a) 3° ≤ 2θ ≤ 70°; b) 2° ≤ 2θ ≤ 25° recorded at higher sensitivity: 1) Na-Wy; 2) AP and 3) CoAP (MM – montmorillonite, Q – quartz and F – feldspar).

Table 1
Chemical composition of samples.

Sample	Oxide content (mass %)						
	SiO_2	Al_2O_3	Fe_2O_3	MgO	Na_2O	CoO	H_2O
Na-Wy	58 ± 3	22 ± 2	4.0 ± 0.8	3.6 ± 1.0	2.6 ± 1.3	< 0.01	9.1 ± 0.1
AP	53 ± 3	28 ± 2	3.6 ± 0.3	3.5 ± 0.7	< 0.01	< 0.01	7.9 ± 0.1
CoAP	57 ± 3	25 ± 3	3.1 ± 0.1	2.3 ± 0.3	< 0.01	3.9 ± 0.3	5.6 ± 0.1

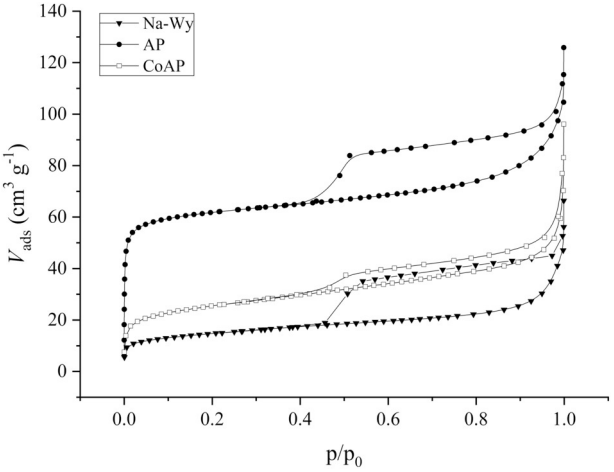

Fig. 2. Low temperature N_2 adsorption-desorption isotherms.

(expressed as 3.9 wt% CoO) might not be sufficient to ensure Co oxides detection in CoAP by XRPD, particularly since they could have been obtained in lower crystallinity forms.

The pillaring process fixed the basal spacing. The test for swelling index (ASTM D5890-19, 2019) also confirmed the loss of swelling property for AP. The obtained basal spacing (1.72 nm for AP) was in accordance with previously reported values (Brotas de Carvalho et al., 1996; Flego et al., 1998) for aluminum pillared montmorillonite originating from Wyoming clay deposits. On the other hand, the 001 montmorillonite reflection in CoAP derogated. Therefore additional XRPD analysis using more sensitive device was performed and the results are shown in Fig. 1b. The d_{001} values were 1.18 nm, 1.72 nm, and 1.53 nm for Na-Wy, AP and CoAP, respectively. According to literature, decreased d_{001} value for CoAP is expected because of repeated calcination at elevated temperature (450 °C) (Gil et al., 2000).

Low temperature N_2 adsorption-desorption isotherms for all investigated samples are given in Fig. 2, while calculated textural parameters according to appropriate models are provided in Table 2.

All isotherms belong to the II type according to the IUPAC and are reversible at lower equilibrium pressures with the H3 type of hysteresis loop for $p/p_0 > 0.4$. These findings are expected for materials consisted of aggregated planar particles and slit type of pores. (Leofanti et al., 1998; Vuković et al., 2005).

The isotherms exhibit significant increase of the amount of adsorbed nitrogen in AP at pressures corresponding to micropores, which is a proof of successful pillaring (Mudrinić et al., 2014). It can be concluded that there was a significant decrease of micropore volume for CoAP, which remained higher with respect to that of Na-Wy.

Such result implies that a part of incorporated cobalt oxide affected the interlamellar space of AP. The decrease of hysteresis in the physisorption curves related to CoAP, in comparison with that of AP, indicates that cobalt oxide was also incorporated within the mesopores, thus dampening the effect of capillary condensation. Detailed information on the obtained textural properties' values is presented in Table 2.

By comparing the results for Na-Wy, AP and CoAP ($\leq$ 2 μm fraction) with those obtained for $\leq$74 μm fraction (Marković et al., 2018), it can be noticed that:

- All the trends obtained for the $\leq$74 μm fraction also occurred in the case of the $\leq$2 μm fraction i.e. textural properties $V_{0.98}$, S_{BET}, V_t and S_{mic} increased in the following order Na-Wy < CoAP < AP,
- The specific surface area was more developed for all the samples obtained from $\leq$2 μm fraction then for the $\leq$74 μm fraction (Marković et al., 2018). This was expected since hydroseparation led to the increase of montmorillonite content and decrease of the accompanying minerals – quartz and feldspar – that have less developed specific area.

Table 2 and Fig. 2 show that cobalt containing phase was incorporated both in the micropores and mesopores, i.e. the interlamellar and interparticle space of the pillared material. Mesopore volume for CoAP decreased, while the corresponding surface area slightly increased, comparing with those of AP, which implies the shift of mesopore diameters to lower values. In order for this conclusion to be tested, the distribution of mesopore diameters, obtained using the Barrett, Joyner, Hallenda method, was investigated (Rouquerol et al., 1999). The distribution diagrams, as acquired by the software, are presented in Supplementary data (Fig. S1). They show that the pillaring resulted in the development of low diameter mesopores and occurrence of new pores within a broad range of mesopore sizes. After cobalt impregnation the most abundant mesopore diameter size, d_{max}, remained unchanged, while the volume and surface area of the pores of about 4.0 nm in diameter dropped to approximately half the value of that for AP. This implies pore filling of pores in AP as the consequence of impregnation. This conclusion is in line with the discussion above regarding physisorption isotherms and probably originates in the filling of higher diameter mesopores, or even macropores, which could not be measured using this method.

The obtained micropore diameter distribution according to the Horvath, Kawazoe method is given in Supplementary data in Fig. S2 (Horvath and Kawazoe, 1983). According to these results the pillaring resulted in the development of micropores. After cobalt impregnation the micropore diameter size distribution remained similar while the surface area of the micropores was dramatically reduced (Table 2), although still higher than that of Na-Wy. This implies that micropores were also filled with cobalt oxide containing phase.

Selected SEM microphotographs of Na-Wy (a), AP (b) and CoAP (c) taken at the same magnification (× 10,000) are presented in Fig. 3.

All samples exhibited layered structure typical for montmorillonite since it is the dominant mineral. The morphology was retained after performed modifications. There was only a decrease in the size of the aggregates caused by modification, which is in accordance with literature data (Metz et al., 2005). The degree of agglomeration decreased in the following order: Na-Wy > AP > CoAP. The EDS analysis of chemical composition was applied in order to confirm XRF results. The results collected using the two methods were in good agreement. The mass percentage of detected elements is given in Table 3.

The presence of cobalt in CoAP was confirmed. The range of

Table 2
Selected textural properties of investigated samples.

Sample	$V_{0.98}$ (cm^3 g^{-1})	V_{mes}^{BJH} (cm^3 g^{-1})	S_{BET} (m^2 g^{-1})	V_t (cm^3 g^{-1})	S_t (m^2 g^{-1})	S_{micr} (m^2 g^{-1})
Na-Wy	0.080	0.072	53	0.010	29	24
AP	0.147	0.082	265	0.078	39	226
CoAP	0.082	0.055	96	0.018	49	36

$V_{0.98}$ – total pore volume (Gurvitch method); V_{mes}^{BJH} volume of mesopores according to the Barrett, Joyner, Halenda method; S_{BET} – specific surface area (Brunauer, Emmett, Teller - 3 parameter equation); V_t and S_t – mesopore volume and mesopore surface area t-Plot (Lippens and de Boer, using universal Harkins, Jura standard isotherm), S_{mic} – specific micropore volume ($S_{BET} - S_t$) (Gregg and Sing, 1967; Rouquerol et al., 1999; Webb and Orr, 1997; Dubinin, 1974; Scherdel et al., 2010).

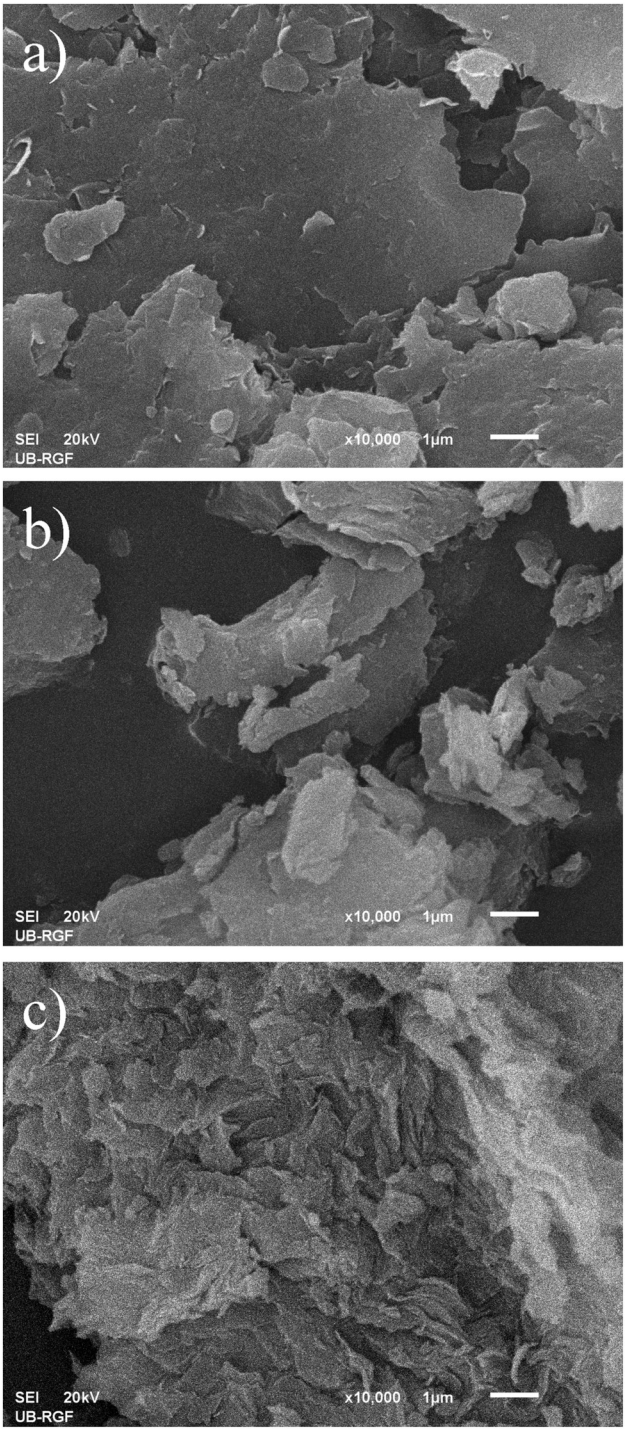

Fig. 3. SEM microphotographs of: a) Na-Wy, b) AP and c) CoAP.

elements to be investigated using EDS was deliberately shrunk to the major constituents and those relevant in the performed modifications. The results are here normalized taking into consideration only the selected set of elements. The results of XPS confirmed the presence of Co^{2+} in the investigated sample in the form of CoO. The characteristic parts of XPS spectrum of CoAP are presented in Fig. S3.

A common conclusion, which can be drawn from the presented characterization results, would be that cobalt was successfully incorporated into AP. Besides, the incorporation was not only superficial, but it affected the bulk of the material, in particular the interlamellar and interparticle space. The incorporated oxide forms probably were not dominantly crystalline and/or their content was not sufficient to be detectable by XRPD.

3.2. Results of catalytic tests

3.2.1. Influence of mass of catalyst

The influence of the mass of catalyst (m_{cat}) was investigated in the range of masses between 5 mg and 200 mg per equal suspension volumes. Decolorization reactions were carried out maintaining equal experimental conditions, i.e. 200 ml of 50 mg dm^{-3} tartrazine solution, 40 mg of Oxone® (0.130 mmol), reaction time of up to 240 min. They were monitored using UV–Vis spectrophotometry. The extent of decolorization was estimated using the peak at 426 nm, characteristic for tartrazine. The results collected at the tenth minute of the reactions are shown (Fig. 4) for two different temperatures: 30 °C and 50 °C.

With the increase of the mass of the catalyst the degree of decolorization increased, which was more prominent at the higher temperature. The increase was nearly linear for both temperatures up to plateau related to 100% of decolorization. At 50 °C, total decolorization occurred after ten minutes for m_{cat} = 100 mg. On the other hand, at 30 °C, only 20% of decolorization was achieved for the same mass of catalyst.

The process of catalytic degradation of tartrazine, aside from decolorization, includes other processes too, reflected in changes in the UV–Vis spectra. Therefore, it was necessary to use lower m_{cat} in the experiments in order to monitor the occurrence and disappearance of some of degradation products, detectable by this method.

The mass of the catalyst of 5 mg was chosen for further experiments.

3.2.2. The influence of temperature

Under experimental conditions reported above, and the amount of catalyst of 5 mg, the influence of temperature was investigated in the (30–70) °C temperature range. Decolorization was monitored through the changes of the absorbance at λ_{max} = 426 nm during 240 min (Fig. 5 and Table 4).

The decolorization of tartrazine under investigated conditions was fast. Temperature increase was beneficial for the dye degradation rate. Under investigated conditions, total decolorization was achieved only in the case of the reaction conducted at 70 °C. At different temperatures, different kinetic models were found to be applicable. The exponential fit was found to be appropriate for higher temperatures (≥ 50 °C). This fit corresponds to the first order kinetics. The first order rate constant

Table 3
Mean values of EDS and XPS analysis.

Sample	Element mass (mean values and standard deviation), %						
		O	Si	Al	Fe	Mg	Co
AP	EDS	58 ± 2	25 ± 1	14 ± 1	2.4 ± 0.3	1.1 ± 0.1	–
CoAP	EDS	57 ± 6	24 ± 3	13 ± 1	2.2 ± 0.4	1.3 ± 0.1	2.2 ± 1.4
	XPS	55 ± 1 (O 1 s)	25 ± 1 (Si 2p)	15 ± 1 (Al 2p)			5.6 ± 1.4 (Co 2p3/2)

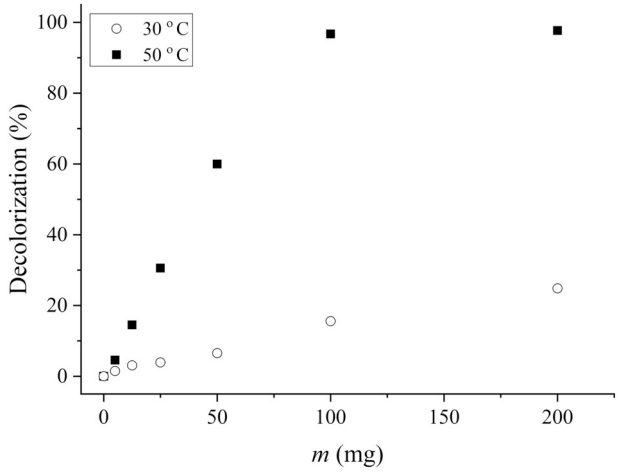

Fig. 4. Influence of mass of catalyst on decolorization of tartrazine at two different temperatures.

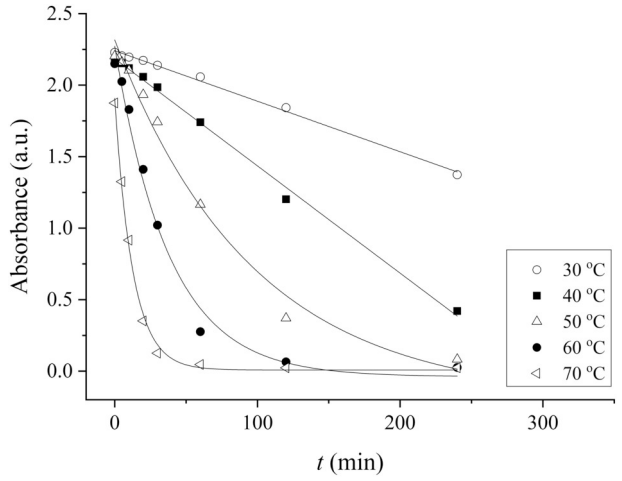

Fig. 5. Decolorization of tartrazine solution monitored at λ_{max} = 426 nm, and at different temperatures, during reaction time.

Table 4
Kinetic models (Lente, 2015) for different reaction temperatures.

Temperature, °C	The best fit equation	R^2
30	$A_t = 2.241–0.00353 \cdot t$	0.996
40	$A_t = 2.185–0.00750 \cdot t$	0.996
50	$A_t = 2.511 \cdot e^{-0.0104t} + 0.182$	0.987
60	$A_t = 2.311 \cdot e^{-0.0263t} - 0.039$	0.989
70	$A_t = 1.899 \cdot e^{-0.0792t} + 0.008$	0.997

t – temperature; A_t – absorbance at temperature t; R^2 – square of coefficient of correlation.

(k) increased with increasing reaction temperature. According to the used model (Lente, 2015) calculated k values were k = 0.0104, 0.0263 and 0.0792 min^{-1} for 50 °C, 60 °C and 70 °C, respectively. Activation energy was calculated to be 93.5 kJ mol^{-1}. The first order kinetics is in agreement with literature data for the degradation of different azo dyes in the presence of peroxide radicals (Beach et al., 2011; Li et al., 2014; Morales et al., 2012; Özen et al., 2005). On the other hand at lower temperatures (at 30 °C and 40 °C) linear fit was applicable for tartrazine decolorization at 426 nm.

In the spectrum of tartrazine aqueous solution (C_0 = 50 mg dm^{-3}) only two distinguished peaks were identified – one at the wavelength (λ_{max}) of 426 nm, originating from chromophore group (yellow color) and the other at λ_{max} = 257 nm related to aromatic ring (Oancea and Meltzer, 2013). At 30 °C, only intensity decrease of these peaks was noticeable. The degradation of individual aromatic rings was slower than that of the chromophore itself.

With reaction temperature increase, new peaks corresponding to the formation of degradation products occurred. The UV–Vis spectra for all investigated temperatures are given in Fig. 6 in order for these phenomena to be illustrated.

The formation of the new peak at 231 nm and the broadening of the peak at 426 nm, followed by the formation of a new peak (at approx. 370 nm), occurred at higher temperatures. At 40 °C this phenomenon was observed only after 240 min, while at 50 °C, 60 °C and 70 °C it was noticeable after 120 min, 60 min, 30 min and 20 min of the reaction, respectively.

A new peak at 275 nm occurred only at elevated temperatures (≥ 50 °C) for longer reaction times and persisted to exist up to 240 min of the reaction. The same applies for the peak at 231 nm. On the other hand the peak at 370 nm disappeared at elevated temperatures during the investigated period of time.

New peaks occurring during the reaction are related to the formation of tartrazine degradation products.

Based on the spectra presented in Fig. 6, the deconvolution of the peaks at 231 nm and 257 nm was performed in order for the change of their intensity to be investigated. The deconvolution was performed using the MagicPlot Pro 2.7.2 software. Different mathematical functions were tested, and the one with the best correlation with the experimental data (having square of coefficient of correlation $R^2 \geq 0.99$) was applied in deconvolution. The results are presented in Fig. 7.

The relative intensity of the peak at 257 nm (Fig. 7a) decreased during the reaction. This decrease was faster for higher reaction temperatures. This peak completely disappeared after 240 min for 60 °C and 70 °C. The formation of a new absorption peak at 231 nm was presented in Fig. 7b. At 40 °C and 50 °C this peak appeared only after 240 min and 120 min respectively. For the reactions conducted at 60 °C and 70 °C it was possible to monitor the appearance and increase of the relative intensity of the peak at 231 nm, followed by its decrease for longer reaction times. During the investigated period of time, this peak did not disappear completely.

3.2.3. *Influence of pH of initial dye solution*

The influence of pH of the initial dye solution on decolorization process (426 nm) was investigated in the pH range from 2 to 11. The experiments were conducted at 50C° and the following process parameters were: C_0 = 50 mg dm^{-3}, V = 200 cm^3, m_{cat} = 5 mg and 1.30 mmol Oxone® per 1 g of catalyst. No shift of chromophore attributed peak at 426 nm was noticed for 2 < pH < 8. Since pKa of tartrazine is 9.4 (Pérez-Urquiza and Beltrán, 2001), the change in the UV–Vis spectra of the dye was expected. Above pKa this peak was shifted to 399 nm. At pH = 11 and under the same experimental conditions, the intensity of peak decreased for not more than approx. 15%. On the other hand, total decolorization occurred for all other investigated initial pH values (Fig. 8). Decolorization analyzed by monitoring the intensity changes of the absorption peak at λ_{max} = 426 nm during time for different initial pH values is presented in Fig. 8.

The reaction was faster for the initial pH values of 6 and 8, then for unadjusted pH and pH = 2. For pH = 6 and pH = 8 decolorization was complete after 120 min, while for the other two pH values complete decolorization was achieved after 240 min. During the reaction, pH value changed, and for the interval of the initial pH values between 3.6 and 8, the final pH value was 3.6. Since pH = 3.6 was the value of the unadjusted pH of the reaction mixture, it seems to be unnecessary for pH to be adjusted before the reaction. In the case of extremely acidic or alkali initial conditions, no change of pH during the reaction occurred.

4. Conclusions

Aluminum pillared clay rich in montmorillonite was impregnated

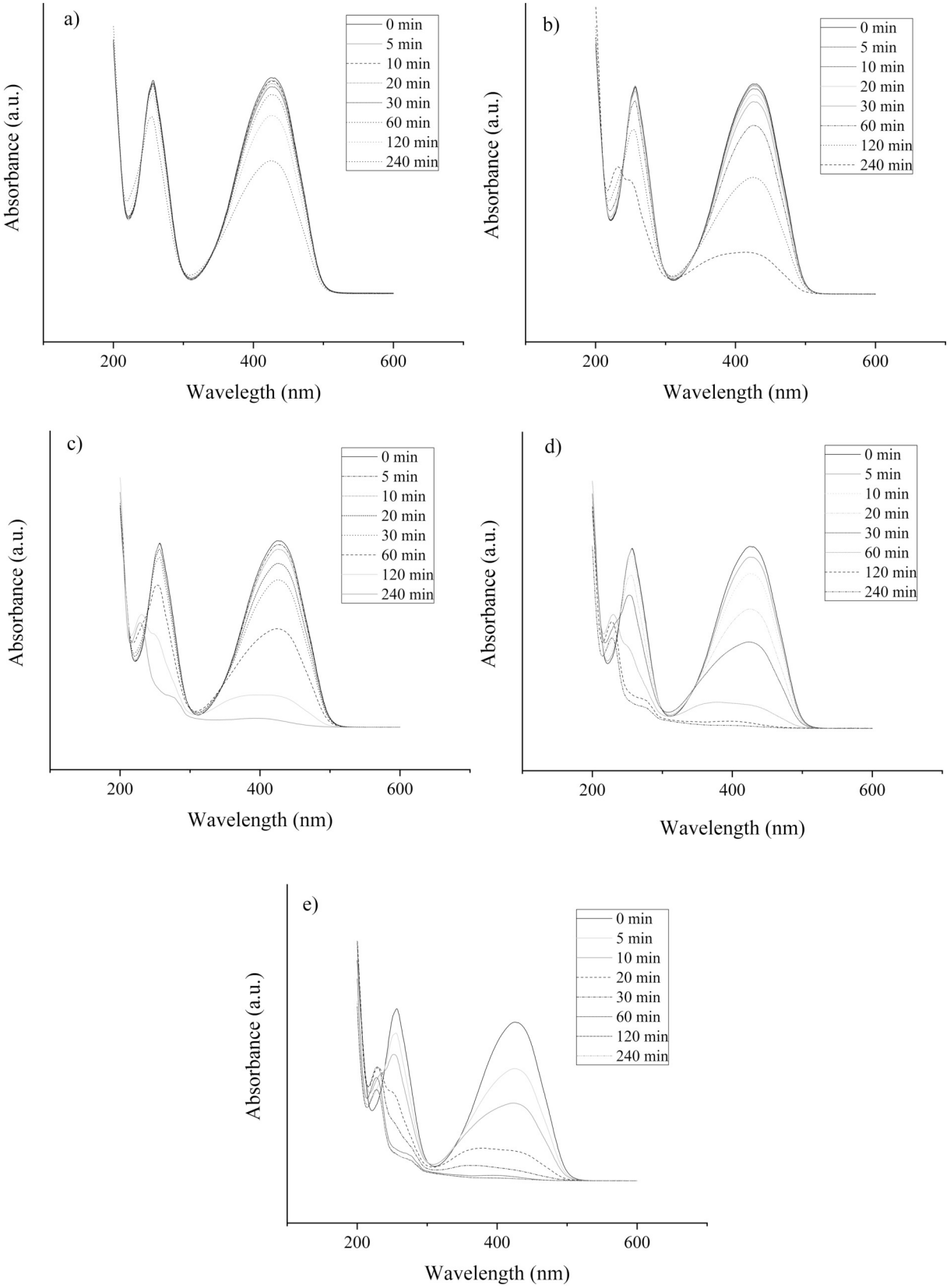

Fig. 6. UV–Vis spectra for catalytic tests with tartrazine (C_0 = 50 mg dm^{-3}, V = 200 cm^3, m_{cat} = 5 mg and 1.30 mmol Oxone® per 1 g of catalyst) performed at: a) 30 °C, b) 40 °C, c) 50 °C, d) 60 °C and e) 70 °C.

with cobalt using the incipient wetness procedure (CoAP). The presence of cobalt in the synthetized material was confirmed by XRF and EDS. The XRPD analysis did not confirm the presence of any forms of crystalline cobalt oxide phases. The amount of cobalt (expressed as 3.9 wt% CoO) was probably not sufficient to be detectable using this method, particularly since cobalt could have been present in less

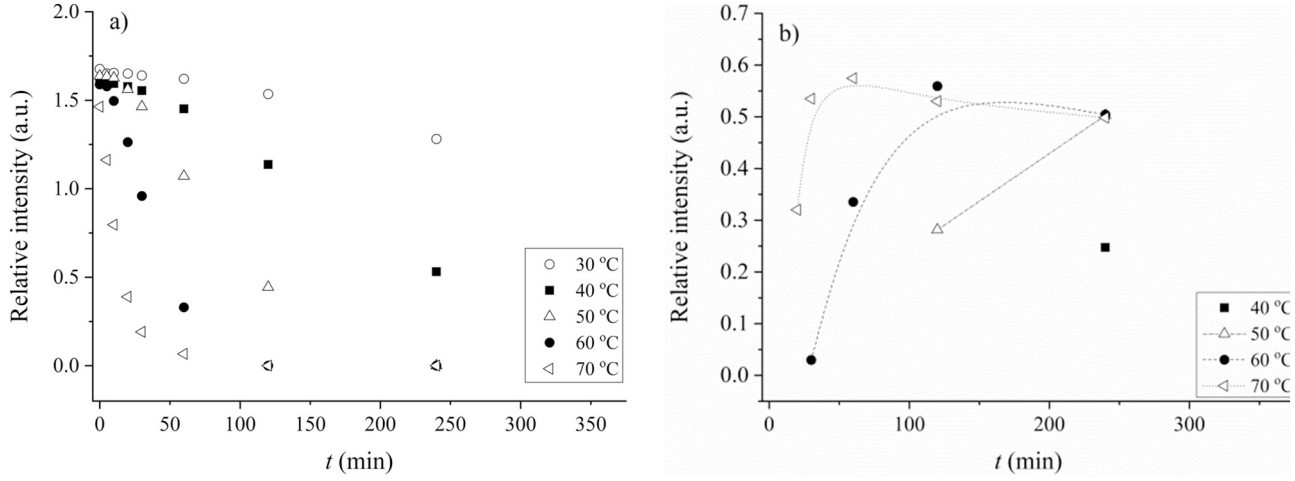

Fig. 7. Relative intensity of deconvoluted peak during the reaction time at different temperatures at λ_{max} values of: a) 257 nm and b) 231 nm.

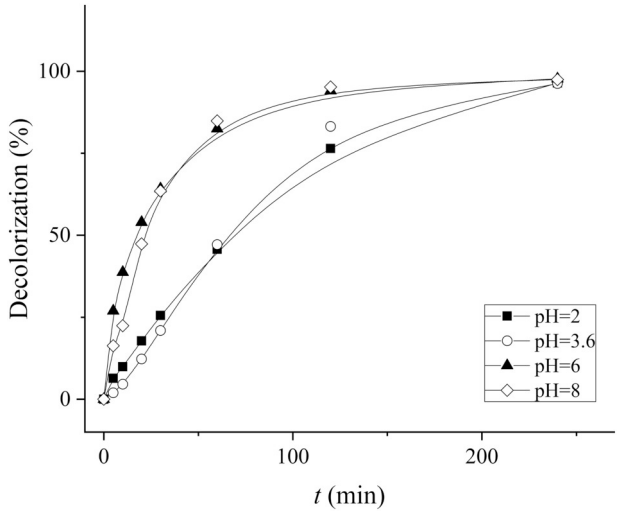

Fig. 8. Decolorization of tartrazine solution monitored at λ = 426 nm during reaction at different initial pH values of the reaction mixture at 50 °C, m_{cat} = 5 mg.

crystalline oxide forms.

Pillaring led to developed meso- and microporosity, while subsequent impregnation resulted in mesopore and micropore filling. This might be regarded as a proof of cobalt oxide incorporation within the pores of aluminum pillared sample (CoAP).

CoAP was tested as catalyst in the activation of radical formation from potassium peroxymonosulfate (Oxone®) in the reaction of oxidative degradation of model dye –tartrazine. UV–Vis spectroscopy was used to monitor decolorization (decrease of chromophore related absorption peak at λ_{max} = 426 nm) and the degradation of aromatic products present in the initial solution and those formed during the reaction. The decolorization of tartrazine under investigated conditions was fast. Temperature increase was beneficial for dye degradation rate. At different reaction temperatures, different kinetic models were found to be applicable. The exponential fit was found to be appropriate for higher temperatures (≥ 50 °C).

UV–Vis spectra were deconvoluted and further analyzed. The peak at 257 nm, originated from aryl moieties, was present in the initial solution while other peaks were attributed to products of the oxidative degradation. The peak at 370 nm occurred during the degradation at higher temperatures and disappeared as the reaction went on.

The relative intensities of the peaks at 257 nm and 231 nm, obtained using deconvolution, were monitored during the reactions conducted at different temperatures. The decrease of the relative intensity of the peak at 257 nm was faster for higher reaction temperatures. The peak at 231 nm was formed during the reaction and was attributed to the formation of degradation products. During the investigated period of time, this peak did not disappear completely.

With the increase of the initial pH of tartrazine/Oxone® system in the range from 2 to 8, the rate of decolorization increased. Above pKa of tartrazine (9.4), the shift of chromophore-attributed peak from 426 nm to 399 nm occurred, and decolorization was significantly less expressed than for lower pH values.

The cobalt impregnated pillared montmorillonite was found to be a promising catalyst for dye decolorization and degradation. It also showed good performance in the degradation of different products formed in tartrazine oxidation in the presence of Oxone®.

Acknowledgement

This work was supported by the Ministry of Education, Science and Technological Development of the Republic of Serbia (Projects III 45001 and ON 176006).

We would like to thank Prof. Dr. Plamen Stefanov, Research Director of Institute of General and Inorganic Chemistry, Bulgarian Academy of Sciences, Sofia, Bulgaria for providing XPS results.

Appendix A. Supplementary data

Supplementary data to this article can be found online at https://doi.org/10.1016/j.clay.2019.105276.

References

Ahmad, M., Teel, A.L., Watts, R.J., 2013. Mechanism of persulfate activation by phenols. Environ. Sci. Technol. 47, 5864–5871.

Ahn, Y.Y., Yun, E.T., Seo, J.W., Lee, C., Kim, S.H., Kim, J.H., Lee, J., 2016. Activation of peroxymonosulfate by surface-loaded noble metal nanoparticles for oxidative degradation of organic compounds. Environ. Sci. Technol. 50, 10187–11097.

Anipsitakis, G.P., Dionysiou, D.D., 2004. Radical generation by the interaction of transition metals with common oxidants. Environ. Sci. Technol. 38, 3705–3712.

Anipsitakis, G.P., Stathatos, E., Dionysiou, D.D., 2005. Heterogeneous activation of oxone using Co_3O_4. J. Phys. Chem. B 109, 13052–13055.

ASTM D5890-19, 2019. Standard Test Method for Swell Index of Clay Mineral Component of Geosynthetic Clay Liners. ASTM International, West Conshohocken, PA.

ATSDR, 1992. Agency for Toxic Substances and Disease Registry (ATSDR). Toxicological Profile for Cobalt, Public Health Service: U.S. Department of Health and Human Services.

Ball, D.L., Edwards, J.O., 1956. The kinetics and mechanism of the decomposition of Caro's acid. J. Am. Chem. Soc. 78, 1125–1129.

Ball, D.L., Edwards, J.O., 1958. The catalysis of the decomposition of caro's acid. J. Phys. Chem. 62, 343–345.

Baloyi, J., Ntho, T., Moma, J., 2018. Synthesis and application of pillared clay

heterogeneous catalysts for wastewater treatment: a review. R. Soc. Chem. 8, 5197–5211.
Beach, E.S., Malecky, R.T., Gil, R.R., Horwitz, C.P., Collins, T.J., 2011. Fe-TAML/hydrogen peroxide degradation of concentrated solutions of the commercial azo dye tartrazine. Catal. Sci. Technol. 1, 437–443.
Brotas de Carvalho, M., Pires, J., Carvalho, A.P., 1996. Characterisation of clays and aluminium pillared clays by adsorption of probe molecules. Micropor. Mater. 6, 65–77.
Chekir, N., Tassalit, D., Benhabiles, O., Kasbadji Merzouk, N., Ghenna, M., Abdessemed, A., Issaadi, R., 2017. A comparative study of tartrazine degradation using UV and solar fixed bed reactors. Int. J. Hydrog. Energy 42, 8948–8954.
Chen, J.D., Yongjian, Y., Show, G., Wang, H., 2018. Activation of peroxymonosulfate by metal (Fe, Mn, Cu and Ni) doping ordered mesoporous Co_3O_4 for the degradation of enrofloxacin. RSC Adv. 8, 2338–2349.
CMS, 2019. Clay Minerals Society, Source Clay Physical/Chemical Data. http://www.clays.org/sourceclays_data.html (accessed March, 20th 2019).
Dubinin, M.M., 1974. On physical feasibility of Brunauer's micropore analysis method. J. Colloid Interface Sci. 46, 351–356.
Durairaj, A., Sakthivel, T., Obadiah, A., Vasanthkumar, S., 2018. Enhanced photocatalytic activity of transition metal ions doped g–C_3N_4 nanosheet activated by PMS for organic pollutant degradation. J. Mater. Sci. 29, 8201–8209.
El-Bahy, Z.M., Mohamed, M.M., Zidan, F.I., Thabet, M.S., 2008. Photo-degradation of acid green dye over Co–ZSM-5 catalysts prepared by incipient wetness impregnation technique. J. Hazard. Mater. 153, 364–371.
Flego, C., Galasso, L., Millini, R., Kiricsi, I., 1998. The influence of the composition on the thermal and acid characteristics of multi-component oxide pillared montmorillonite. Appl. Cat. A General 168, 323–331.
Gil, A., Gandía, L.M., Vicente, M.A., 2000. Recent advances in the synthesis and catalytic applications of pillared clays. Catal. Rev. Sci. Eng. 42, 145–212.
Gil, A., Korili, S.A., Vicente, M.A., 2008. Recent advances in the control and characterization of the porous structure of pillared clay catalysts. Catal. Rev. Sci. Eng. 50, 153–221.
Gregg, S.H., Sing, K.S., 1967. Adsorption, Surface Area and Porosity. Academic Press, New York.
Gržetić, I., Orlić, J., Radić, V., Radić, M., Ilijević, K., 2016. Analysis of medieval Serbian silver coins from XIV and XV century by means of wavelength-dispersive X-ray spectrometry. Nucl. Instrum. Meth. B 366, 161–170.
Hajjaji, W., Pullar, R.C., Labrincha, J.A., Rocha, F., 2016. Aqueous Acid Orange 7 dye removal by clay and red mud. Appl. Clay Sci. 126, 197–206.
Herney-Ramírez, J., Madeira, L.M., 2010. Use of pillared clay-based catalysts for wastewater treatment through Fenton-like processes. In: Pillared Clays and Related Catalysts. Springer, New York, pp. 129–165.
Horvath, G., Kawazoe, K., 1983. Method for the calculation of effective pore size distribution in molecular sieve carbon. J. Chem. Eng. Japan 16, 470–475.
Hu, P., Long, M., 2016. Cobalt-catalyzed sulfate radical-based advanced oxidation: a review on heterogeneous catalysts and applications. Appl. Catal. B Environ. 181, 103–117.
Huang, T., Chen, J., Wang, Z., Guo, X., Crittenden, J.C., 2017. Synthesis and application of pillared clay heterogeneous catalysts for wastewater treatment: a Review. Environ. Sci. Pollut. Res. 24, 9651–9661.
Jain, R., Bhargava, M., Sharma, N., 2003. Electrochemical studies on a pharmaceutical azo dye: tartrazine. Ind. Eng. Chem. Res. 42, 243–247.
JCPDS, 1990. International Center for Diffraction Data. Joint Committee on Powder Diffraction Standards (JCPDS), Swarthmore, USA, pp. 1990.
Kaloidas, V., Koufopanos, C.A., Gangas, N.H., Papayannakos, N.G., 1995. Scale-up studies for the preparation of pillared layered clays at 1 kg per batch level. Micropor. Mater. 5, 97–106.
Khelifi, S., Ayari, F., Hassan Chehimi, D.B., Trabelsi-Ayadi, M., 2016. Synthesis and characterization of heterogeneous catalysts and comparison to iron-ore. J. Chem. Eng. Process Technol. 7, 1–9.
Kommineni, S., Zoeckler, J., Stocking, A., Liang, S., Flores, A., Kavanaugh, M., 2008. Perspective Advanced oxidation processes for water treatment: advances and trends for R&D. J. Chem. Technol. Biotechnol. 83, 769–776.
Lente, G., 2015. Deterministic Kinetics in Chemistry and Systems Biology. The Dynamics of Complex Reaction Networks. Springer Briefs in Molecular Science, New York.
Leofanti, G., Padovan, M., Tozzola, G., Venturelli, B., 1998. Surface area and pore texture of catalysts. Catal. Today 41, 207–219.
Li, M., He, W., Liu, Y., Wu, H., Wamer, W.G., Lo, Y.M., Yin, J.J., 2014. FD&C Yellow No. 5 (Tartrazine) Degradation via reactive oxygen species triggered by TiO_2 and Au/TiO_2 nanoparticles exposed to simulated sunlight. J. Agric. Food Chem. 62, 12052–12060.
Lin, K.Y.A., Lin, T.Y., 2018. Degradation of acid azo dyes using oxone activated by cobalt titanate perovskite. Water Air Soil Pollut. 229, 10.
Lin, K.Y.A., Lin, J.T., Lu, X.Y., Hung, C., Lin, Y.F., 2017. Electrospun magnetic cobalt-embedded carbon nanofiber as a heterogeneous catalyst for activation of oxone for degradation of Amaranth dye. J. Colloid Interface Sci. 505, 728–735.
Lin, K.Y.A., Tong, W.C., Du, Y., 2018. Cobalt-embedded carbon nanofiber derived from a coordination polymer as a highly efficient heterogeneous catalyst for activating oxone in water. Chemosphere 195, 272–281.
Marković, M., Marinović, S., Mudrinić, T., Mojović, Z., Ajduković, M., Milutinović-Nikolić, A., Banković, P., 2018. Cobalt impregnated pillared montmorillonite in the peroxymonosulfate induced catalytic oxidation of tartrazine. React. Kinet. Mech. Catal. 125, 827–841.
Metz, V., Amram, K., Ganor, J., 2005. Stoichiometry of smectite dissolution reaction. Geochim. Cosmochim. Acta 69, 1755–1772.
Mishra, T., 2010. Transition Metal Oxide-Pillared Clay Catalyst: Synthesis to Application. In: Pillared Clays and Related Catalysts. Springer, New York, pp. 99–128.
Morales, G.V., Sham, E.L., Cornejo, R., Torres, E.M.F., 2012. Kinetic studies of the photocatalytic degradation of tartrazine. Lat. Am. Appl. Res. 42, 45–49.
Mudrinić, T., Mojović, Z., Milutinović-Nikolić, A., Banković, P., Dojčinović, B., Vukelić, N., Jovanović, D., 2014. Beneficial effect of Ni in pillared bentonite based electrodes on the electrochemical oxidation of phenol. Electrochim. Acta 114, 92–99.
Nfodzo, P., Choi, H., 2011. Triclosan decomposition by sulfate radicals: Effects of oxidant and metal doses. Chem. Eng. J. 174, 629–634.
Oancea, P., Meltzer, V., 2013. Photo-Fenton process for the degradation of tartrazine (E102) in aqueous medium. J. Taiwan Inst. Chem. Eng. 44, 990–994.
Oh, W.D., Dong, Z., Lim, T.T., 2016. Generation of sulfate radical through heterogeneous catalysis for organic contaminants removal: current development, challenges and prospects. Appl. Catal. B Environ. 194, 169–201.
Özen, A.S., Aviyente, V., Tezcanli-Güyer, G., Ince, N.H., 2005. Experimental and modeling approach to decolorization of azo dyes by ultrasound: degradation of the hydrazone tautomer. J. Phys. Chem. A 109, 3506–3516.
Pérez-Urquiza, M., Beltrán, J.L., 2001. Determination of the dissociation constants of sulfonated azo dyes by capillary zone electrophoresis and spectrophotometry methods. J. Chromatogr. A 917, 331–336.
Pinna, F., 1998. Supported metal catalysts preparation. Catal. Today 41, 129–137.
Rouquerol, F., Rouquerol, J., Sing, K., 1999. Adsorption by Powders and Porous Slides. Academic Press, London.
Scherdel, C., Reichenauer, G., Wiener, M., 2010. Relationship between pore volumes and surface areas derived from the evaluation of N2-sorption data by DR-, BET- and t-plot. Microporous Mesoporous Mater. 132, 572–575.
Shukla, P., Sun, H., Wang, S., Ang, H.M., Tadé, M.O., 2011. Co-SBA-15 for heterogeneous oxidation of phenol with sulfate radical for wastewater treatment. Catal. Today 175, 380–385.
Thermofisher, 2019a. OXSAS™ X-ray Fluorescence Analytical Software. https://www.thermofisher.com/order/catalog/product/IQLAAHGABUFABXMATY (accessed August, 19th 2019).
Thermofisher, 2019b. Thermo Scientific UniQuant. https://tools.thermofisher.com/content/sfs/brochures/XR-PS41207-UniQuant-1113.pdf (accessed August, 19th 2019).
Verma, S., Nakamura, S., Sillanpää, M., 2016. Application of UV-C LED activated PMS for the degradation of anatoxin-a. Chem. Eng. J. 284, 122–129.
Vuković, Z., Milutinović-Nikolić, A., Krstić, J., Abu-Rabi, A., Novaković, T., Jovanović, D., 2005. The influence of acid treatment on the nanostructure and textural properties of bentonite clays. Mater. Sci. Forum 494, 339–344.
Webb, P.A., Orr, C., 1997. Analytical Methods in Fine Particle Technology. Micromeritics Instrument Corporation, Norcross, USA.
Yang, Q., Choi, H., Dionysiou, D.D., 2007. Nanocrystalline cobalt oxide immobilized on titanium dioxide nanoparticles for the heterogeneous activation of peroxymonosulfate. Appl. Catal. B Environ. 74, 170–178.
Yang, Q., Choi, H., Chen, Y., Dionysiou, D.D., 2008. Heterogeneous activation of peroxymonosulfate by supported cobalt catalysts for the degradation of 2,4-dichlorophenol in water: the effect of support, cobalt precursor, and UV radiation. Appl. Catal. B Environ. 77, 300–307.
Yang, Y., Jiang, J., Lu, X., Ma, J., Liu, Y., 2015. Production of sulfate radical and hydroxyl radical by reaction of ozone with peroxymonosulfate: a novel advanced oxidation process. Environ. Sci. Technol. 49, 7330–7339.